


Independently Reconfigurable Internal Loss and Resonance Shift in an Interferometer-Embedded Optical Cavity

Aneesh Dash[✉],* Viphretuo Mere[✉], S.K. Selvaraja[✉], and A.K. Naik[✉]†

Centre for Nano Science and Engineering, Indian Institute of Science, Bangalore 560012, India

 (Received 1 November 2021; revised 22 June 2022; accepted 19 September 2022; published 10 November 2022)

Optical cavities find diverse uses in lasers, frequency combs, optomechanics, and optical signal processors. Complete reconfigurability of the resonant frequency as well as the loss enables development of generic field programmable cavities for achieving the desired performance in these applications. Conventional reconfigurable cavities are generally limited to specific material platforms or specific optical tuning methods and require sophisticated fabrication. Furthermore, the tuning of the loss is coupled to the resonance shift in the cavity. We propose and demonstrate a simple and generic interferometer in a cavity structure that enables quasiperiodic modification of the internal cavity loss and the cavity resonance to reconfigure the Q factor, transmission characteristics, and group delay of the hybrid cavity, with simple tuning of the optical phase in the interferometer. We also demonstrate methods to decouple the tuning of the loss from the resonance shift, that enables resonance-locked reconfigurability. This structure also enables resonance shift to both shorter and longer wavelengths using the same phase-tuning technique, which is challenging to achieve in conventional reconfigurable cavities. These devices can be implemented in any guided-wave platform (on-chip or fiber-optic) with potential applications in programmable photonics and reconfigurable optomechanics.

DOI: [10.1103/PhysRevApplied.18.054032](https://doi.org/10.1103/PhysRevApplied.18.054032)

I. INTRODUCTION

Optical cavities are ubiquitous in modern technology, such as lasers [1,2], frequency combs [3], nonlinear optics [4,5], optomechanics [6–11], sensing [12,13], signal processing [14], computing [15,16], and communication [17]. The resonant frequency of an optical cavity depends on the effective refractive index (real part) experienced by the light inside the cavity, while the cavity loss depends on the optical losses inside the cavity as well as the losses at the input-output couplers. Reconfiguring both the resonant frequency and the loss in an optical cavity is useful in programmable optical circuits and photonic computing [18–24] to extract the desired performance from the cavity. Tuning the cavity resonance is readily achieved by phase-tuning (change in real part of the effective refractive index) methods like thermo-optic [25–27], electro-optic [28–30], or all-optical methods [31,32]. Applications such as cavity optomechanics, optical delay lines and memories, where the photon lifetime in the cavity plays an important role, require reconfigurable cavity loss [33–38]. However, reconfiguration of the optical loss in the cavity is restricted to specific tuning methods, device structures, or material platforms [39]. Such techniques involve operation at high optical intensities [31], high electric fields [39],

integration of electroabsorption materials [28,29] or thermally activated phase-change materials [40,41]. Most of these approaches are not generic to all photonic material platforms or optical tuning techniques [39]; integration of other materials is often inherently lossy and significantly alters the optical mode in the cavity, limiting the applications of these optical cavities. It is therefore desirable to have a generic reconfigurable optical cavity that can work on any photonic material platform with any phase-tuning approach.

One such class of reconfigurable optical cavity involves tuning the input-output coupling to the cavity using a thermo-optically or optomechanically tunable coupler, which alters the external losses and reconfigures the loaded quality factor (Q) of the cavity [19,22,42–46]. In these methods involving a single coupler, precise control over the tuning is challenging. A simpler and more efficient solution is to use an interferometer as a distributed coupler into the cavity [33–35]. In this two-point coupled optical cavity structure, tuning the phase difference between the two arms of the interferometer creates a controlled change in the effective power coupled into (or leaking out of) the cavity, thus modifying the coupling and the loaded Q . This structure has been successfully employed in photonic integrated circuits for various signal-processing applications, where significant changes in the cavity transmission are required [33–35]. However, the standalone input-output relation of the optical cavity is inevitably altered in this

*aneesh@iisc.ac.in

†anaik@iisc.ac.in

approach (see Supplemental Material [47]). Many applications such as cavity optomechanics, quantum optics, photonic cavity molecules (higher-order optical cavities) treat the optical cavity as a standalone structure and the input-output coupling is effected by generic methods such as a tapered optical fiber or point and racetrack coupled waveguides [6–11,48]. The presence of the interferometer at the coupler limits the cavity’s usage in such applications. In these applications, it is useful to tune the internal Q of the cavity, instead of the loaded Q , so that the reconfigurable optical cavity can be treated as a standalone entity independent of the coupler. A generic phase-tuning approach for both internal loss and resonance shift, that can be applied on any photonic platform, would be extremely useful to achieve full reconfigurability of an optical cavity. An ideal reconfigurable cavity is expected to allow independent control over the resonant frequency and the cavity loss, that has remained a challenge using the conventional approaches. This work demonstrates such an optical cavity.

In our work, we embed a geometrically balanced Mach-Zehnder interferometer (MZI) within the optical cavity (a microring resonator). In contrast to the interferometric coupler, this implementation tunes the internal loss (or internal Q) of the cavity by modulating the power lost to the radiation modes during interference (when the waves in the two arms recombine) within the cavity. We show that the interferometer-embedded microring resonator (IMRR) structure readily achieves similar desirable changes in the cavity transmission as the two-point coupled microring resonator [33–35]. The simple reconfiguration from an undercoupled cavity to an overcoupled cavity allows for tuning and switching the cavity delay between optical delay (negative) and optical advance (positive). In addition, we observe a wide variety of quasiperiodic changes of both the resonant wavelength and the cavity loss at different interferometer configurations. Such reconfigurability allows us to induce both blueshift and redshift in the cavity resonance with the same phase-tuning technique in the same photonic platform. The cavity structure is general to any traveling-wave optical cavity implemented in optical fibers or integrated photonic platforms and any phase-tuning technique can be used to achieve the desired reconfigurability. Our structure enables reconfiguration of the cavity loss without shifting the resonance for resonance-locked operation [18], which is the goal for an ideal reconfigurable cavity. These fully reconfigurable optical cavities open unexplored avenues in optical memories and cavity optomechanics.

II. INTERFEROMETER-EMBEDDED MICRORING RESONATOR

Phase tuning involves, tuning the refractive index (real part) of the optical medium. The resultant change in the

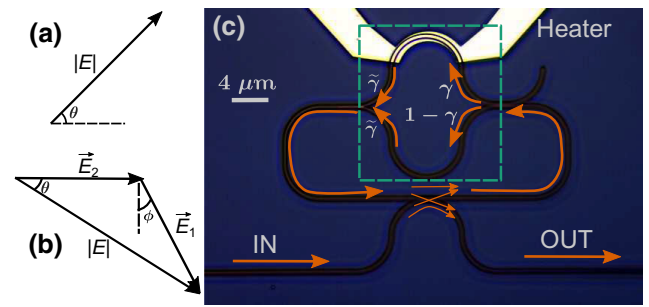


FIG. 1. (a) Phasor illustration of phase tuning in an ordinary optical cavity (\vec{E} denotes the field in the cavity). (b) Phasor illustration of phase tuning in an interferometer-embedded optical cavity ($\vec{E}_{1,2}$ denote the fields in the top and bottom arm of the interferometer, respectively). (c) Optical micrograph of the interferometer-embedded microring resonator (highlighted section shows the MZI).

phase of the electric field of the propagating wave is illustrated in Fig. 1(a); the magnitude of the transmitted field does not change. On the other hand, phase tuning in one arm of a MZI, while leaving the phase of the other arm unchanged, tunes both the magnitude and phase of the resultant field, as shown in Fig. 1(b). Thus, a MZI converts pure phase tuning to loss tuning in the transmitted wave. We utilize this effect to realize phase-reconfigurable loss in an optical cavity.

We demonstrate the working of this modified optical cavity, using the IMRR structure implemented on a silicon-on-insulator (SOI) platform as shown in Fig. 1(c). The details of the fabrication of the devices can be found within the Supplemental Material [47]. The MZI (highlighted) is embedded in the closed path of the microring resonator (MRR). The waveguides have a cross section of $450 \times 220 \text{ nm}^2$ and operate in the fundamental quasi-TE mode in the 1550–1600 nm wavelength range. The bus waveguide is directionally coupled to the cavity. The geometrical round-trip length of the cavity $L = 184 \mu\text{m}$, of which the MZI covers $l = 63 \mu\text{m}$; both arms of the MZI are equal in length. The splitter of the MZI is realized using a directional coupler with power splitting ratio $\gamma : (1 - \gamma)$. The combiner is realized using a Y junction, that combines an equal power fraction $\tilde{\gamma}$ from each arm with an overall insertion loss of 0.5 dB in our design [49]. We note that this loss is a limitation of our implementation, but not of the IMRR structure. The combiner could also be realized using a directional coupler to achieve additional design flexibility, with some optical power tapping out of the cavity into a drop port. The phase tuning is implemented using Ti/Pt heaters that are above the waveguides with an SiO_2 spacer of $1 \mu\text{m}$ thickness to avoid unwanted optical absorption by the metal. We study many such devices with multiple bus-cavity coupling and multiple splitting ratios of the MZI.

The field transmission $[t(\omega)]$ at a frequency ω to the through port of an optical cavity is given by [14]

$$t(\omega) = 1 - \frac{\kappa_{\text{coup}}}{j(\omega - \omega_0) + \kappa_{\text{loss}}/2 + \kappa_{\text{coup}}/2}, \quad (1)$$

where κ_{coup} is the bus-cavity coupling and κ_{loss} is the internal loss; the resonant frequency $\omega_0 = 2\pi c/\lambda_{\text{res}}$, where λ_{res} is the resonant wavelength and c is speed of light in vacuum. In our modified cavity, the loss and the resonant frequency can be expressed as (see Supplemental Material for the derivation [47])

$$\kappa_{\text{loss}} = \frac{v_g}{L} [\zeta L - \ln \tilde{\gamma} - \ln(1 + 2\sqrt{\gamma(1-\gamma)} \sin \phi)], \quad (2)$$

$$\lambda_{\text{res}} = \frac{n_{\text{eff}} L}{m + \frac{1}{2\pi} \arctan\left(\frac{\cos \phi}{\sqrt{(1-\gamma)/\gamma} + \sin \phi}\right)}, \quad (3)$$

where ζ is the fractional propagation loss per unit length in the cavity and ϕ is the tunable phase difference between the top and bottom arms of the MZI; m is the resonance order. It can be seen from Eqs. (2) and (3) that both cavity loss and resonant wavelength can be reconfigured with ϕ , which is the result of embedding the MZI in the cavity. We tune ϕ thermo-optically using the Ti/Pt heaters [26] and record the input-output transmission spectra of the devices using a tunable-laser source at the input and a photodetector at the output.

III. PHASE-TUNABLE INTERNAL LOSS AND RESONANCE SHIFT

When the cavity is reconfigured from an undercoupled condition ($\kappa_{\text{coup}} < \kappa_{\text{loss}}$) or overcoupled condition ($\kappa_{\text{coup}} > \kappa_{\text{loss}}$) to critical coupling ($\kappa_{\text{coup}} \approx \kappa_{\text{loss}}$), the extinction ratio (ER) reaches a maximum [14,50]. Figure 2(a) shows the phase-reconfigured transmission of an IMRR with a 50 : 50 power splitter ($\gamma = 0.5$); the legends show the values of ϕ proportional to the heater power (the heater efficiency is estimated as 0.024π rad/mW using the method described in the Supplemental Material [47]). The cavity is reconfigured from an initially undercoupled condition to critical coupling and back by tuning ϕ with the heater. The extracted ER and Q factor are shown in the inset of Fig. 2(a); the dashed line corresponds to the critical point. At critical coupling, the ER is maximum as expected, with an overall change from 0 to 30 dB. An overall five-fold change in Q factor [$Q = \omega_0/(\kappa_{\text{loss}} + \kappa_{\text{coup}})$] from 2000 to 10000 is observed, which is due to the change in $\kappa_{\text{loss}} + \kappa_{\text{coup}}$. The extracted values of κ_{loss} and κ_{coup} [using Eq. (1)] are shown in Fig. 2(b). Since κ_{coup} is independent of ϕ , the Q factor follows the change in κ_{loss} as a

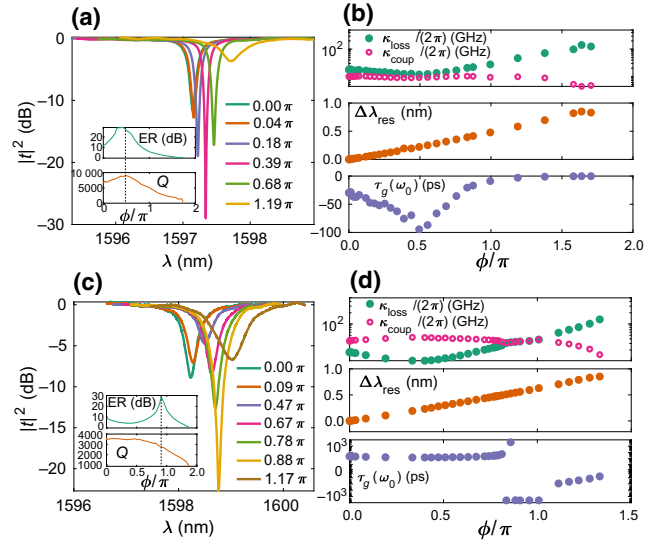


FIG. 2. (a) Thermo-optically reconfigured input-normalized transmitted power response (experimental) for an IMRR with equal power in both arms ($\gamma = 0.5$) and an initial undercoupled condition at different phase shifts ϕ ; inset shows extracted ER and Q factor with the critical point marked by the dashed line, (b) extracted internal loss (κ_{loss}), resonance shift ($\Delta\lambda_{\text{res}}$), and group delay (τ_g in logarithmic scale), (c),(d) similar results for an initially overcoupled cavity.

function of ϕ . The crossover between κ_{loss} and κ_{coup} indicates the critical coupling condition. Using the estimated phase responses $[\Phi(\omega) = \angle t(\omega)]$ from Eq. (1), the group delay ($\tau_g = -d\Phi/d\omega$) at resonance ($\omega = \omega_0$) is shown in Fig. 2(b). At critical coupling, the phase response is the sharpest, resulting in maximal group delay, where negative sign indicates delay [51–54]. The redshifted resonant wavelength (λ_{res}) is shown in Fig. 2(b).

Similar responses for an initially overcoupled cavity are shown in Figs. 2(c)–2(d). In this case, it is observed that κ_{loss} is tuned from slight overcoupling to large overcoupling (causing degradation in ER) and then to a crossover indicating critical coupling (maximal ER) and finally to undercoupling (ER degrades from the maximum). The observations at critical coupling remain unchanged. However, the overcoupled region has an opposite slope of the phase response, resulting in positive values of τ_g , indicating group advance instead of delay [51–54]. Thus the IMRR can be used to reconfigure the cavity between undercoupled and overcoupled conditions through a critical coupling point, to achieve the desired reconfiguration of ER, Q factor, and τ_g .

When $\gamma \approx 0.5$, the tuned λ_{res} has monotonic redshift with ϕ [with expected discontinuities at $\Delta\phi = (4m - 1)\pi/2$ for integer values of m]. This can be readily understood by rotating one of the phasors (of equal length) in Fig. 1(b). On the other hand, cavities with $\gamma \leq 0.5$ [phasors of unequal length in Fig. 1(b)] allow for continuous

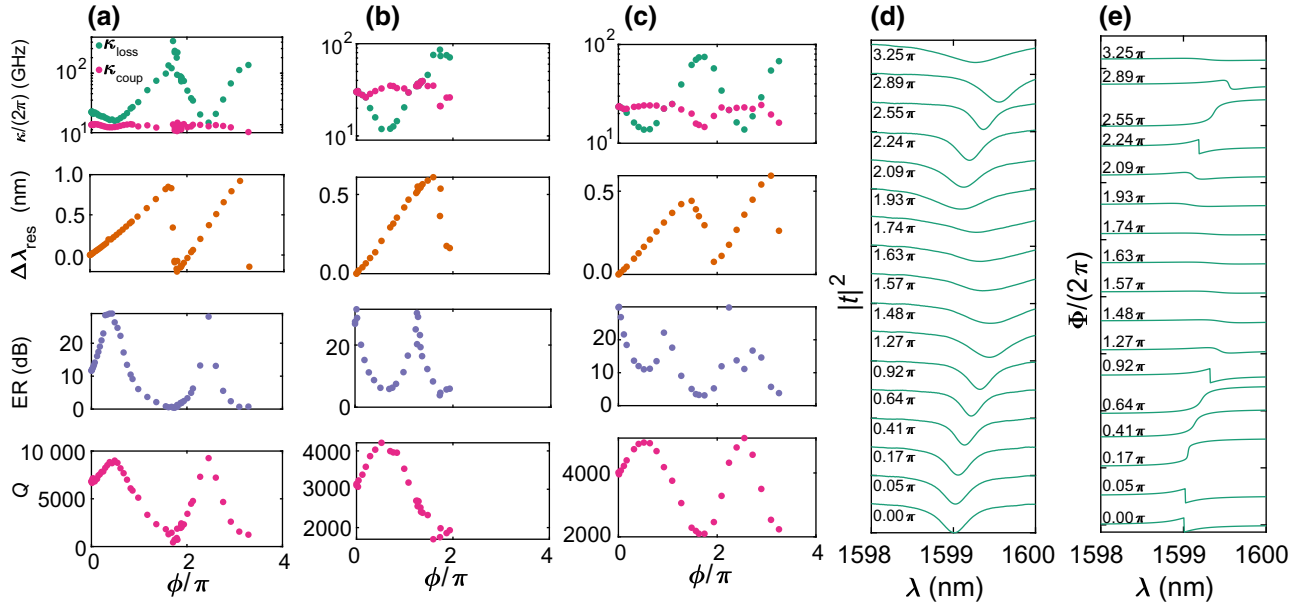


FIG. 3. (a)–(c) Quasiperiodic variations in $\kappa_{\text{loss,coup}}$ (logarithmic scale), λ_{res} , ER, and Q (extracted from experimental data) for $\gamma = 0.5, 0.3, 0.2$, respectively, with ϕ : the blueshift is more gradual for smaller γ . (d),(e) Input-normalized transmitted power response (measured) and phase response (extracted from experimental data) for $\gamma = 0.2$ at different thermo-optically tuned ϕ (responses vertically offset for clarity).

quasiperiodic tuning of both κ_{loss} and λ_{res} . We show the quasiperiodic tuning of the loss and resonant wavelength of three cavities ($\gamma = 0.5, 0.3, 0.2$) at various values of ϕ in Fig. 3; the complete set of transmission responses for the three devices can be found within the Supplemental Material [47]. The quasiperiodic tuning enables estimation of ϕ in Figs. 2 and 3, as outlined in the supplementary information [47]. We note that the quasiperiodicity observed in Fig. 3 deviates from the perfect periodicity expected from Eqs. (2) and (3). We believe such a deviation is due to the wavelength dispersion of the silicon waveguides and directional-coupler based splitters, and also due to stray heat transfer from the heater to the nearby directional couplers and the rest of the optical cavity. Such effects can be reduced by using low-dispersion waveguide platforms such as silicon nitride, broadband directional couplers, and local electro-optic or thermo-optic (with thermal isolation) phase tuners [25].

We track a single resonance in each of the cavities; the free spectral range (FSR) of all the optical cavities is approximately equal to 2.6 nm. For the three cavities, we observe multiple transitions between undercoupled and overcoupled conditions through critical points, whose effect, similar to Fig. 2, is evident in Figs. 3(a)–3(c); the data in Fig. 3(a) is from the same device as Figs. 2(a)–2(b). A peculiar observation in the cavities with $\gamma = 0.3$ and $\gamma = 0.2$ is that λ_{res} has a tunable redshift followed by blueshift. Such a blueshift does not occur for $\gamma = 0.5$; instead a sudden jump in resonant wavelength is observed in Fig. 3. The quasiperiodic resonance shift is clearly

illustrated with the normalized transmission responses for $\gamma = 0.2$ in Fig. 3(d); the corresponding phase responses are shown in Fig. 3(e). Conventional integrated photonic platforms such as silicon and silicon nitride have positive thermo-optic coefficient and hence, thermo-optic tuning allows only for redshift of the cavity resonance [25]. However, with the IMRR structure we achieve both thermo-optic blueshift and redshift in a silicon photonic cavity. Since the IMRR structure is generic to all phase-tuning methods such as electro-optic, all-optic, thermo-optic, etc., any phase tuning in any material platform can result in regions of both redshift and blueshift. Such previously unexplored tuning is extremely useful in reconfigurable photonics and photonic signal processing.

IV. INDEPENDENTLY RECONFIGURABLE INTERNAL LOSS AND RESONANCE SHIFT

For applications such as photonic computing and signal processing, it is desirable to selectively tune the cavity loss without shifting the resonant wavelength [18]. In the IMRR, this can be achieved by phase tuning both the arms of the MZI, as illustrated in Fig. 4(a) where the resultant field has the same phase (θ_0) but different magnitudes depending on the phases ϕ and δ ; the required relation between ϕ and δ (derivation present within the Supplemental Material [47]) is given as

$$\sin(\theta_0 + \delta) = \frac{\sin \theta_0}{\cos(\theta_0 + \phi_0)} \cos(\theta_0 + \phi). \quad (4)$$

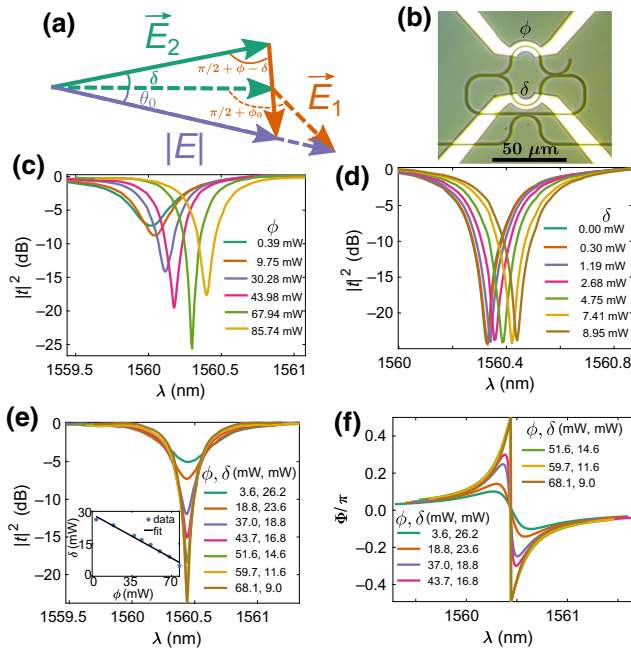


FIG. 4. (a) Phasor illustration of the resonance-locked loss tuning by rotating both phasors simultaneously. (b) Optical micrograph of the IMRR with one heater on each arm of the MZI. Normalized transmitted optical power (experimental) at different phase tuning (heater powers in legends), (c) only at the top heater, (d) only at the bottom heater. (e) Normalized transmitter optical power (experimental) showing resonance-locked thermo-optic reconfiguration of ER and Q factor; inset shows linear relationship between the powers applied at the two heaters, (f) transmitted phase response (extracted from the transmitted optical power).

We implement such phase tuning by placing a heater on each arm of the MZI as shown in Fig. 4(b). The spectra acquired by tuning only the top heater and only the bottom heater are shown in Figs. 4(c)–4(d), respectively. The legends state the applied power at the top and bottom heaters that are proportional to ϕ and δ , respectively; accurate phase estimation (as in Figs. 2 and 3) is not possible for the particular heaters used in the device, since we do not tune over a complete period of λ_{res} and κ_{loss} . We observe that while phase tuning in the top arm changes both λ_{res} and κ_{loss} , only λ_{res} is tuned using the bottom arm; it is similar to an ordinary MRR because for $\gamma = 0.2$, 80% of the optical power travels in the bottom arm that is tuned and the interferometer has negligible effect on the field. When both the heaters are in operation, the resonance can be locked at a particular λ_{res} , while κ_{loss} can be tuned to achieve change in ER, Q factor, and transmitted phase response. Figures 4(e)–4(f) show the normalized transmission and phase response when the resonance shift is suppressed; the heater powers of the top and bottom heater, respectively, are mentioned in the legends. It is observed that the heater powers have a linear relationship (in the limits of small

angles in Fig. 4), as shown in the inset of Fig. 4(e). Hence, a feedback control loop can be used to lock the cavity resonance, while reconfiguring the internal loss. Furthermore, the linear relation can also be used to control both the heaters using a single voltage supply for simpler operation. This provides us a unique method to tune the Q factor, group delay, and ER of the cavity, while always operating at the resonance.

We compare the demonstrated capabilities of our structure to the demonstrations using other structures used in reconfigurable photonics such as reconfigurable Bragg gratings [18] and two-point coupled microring resonators [33–35] in Table I. In comparison to the reconfigurable Bragg gratings [18], our work demonstrates control of internal dissipation in the cavity, is generic to the type of phase-tuning approach and material that can be used, and has less fabrication overhead. The advantage offered by our approach is that the number of control knobs (electrodes for thermo-optic or electro-optic tuning) that need to be simultaneously controlled are two and can be reduced to one, since the two optical phases are related [as shown in Eq. (4) and the inset of Fig. 4(e)]. Since the dependence is approximately linear in the regime of operation used in our experiments, a single electrical input with a divider circuit can be used to simultaneously control the phases in the two arms. Another consequent advantage is the possibility of implementing a closed-loop feedback for stabilizing the cavity resonance while controlling the dissipation.

The two-point coupled microring resonator [33–35] can also achieve similar results as Fig. 4(e) (see theoretical results within the Supplemental Material [47]). However, it cannot achieve the results shown in Fig. 4(f), due to the presence of an unavoidable broadband phase shift with the tuned phases of the interferometer arms. This is a consequence of the placement of the interferometer at the bus-cavity coupler. In our structure, the phase response does not have a background (broadband) shift when the phases in the interferometer arms are altered. On the other hand, in the two-point coupled microring resonator [33–35], the interferometer itself is the coupler to the optical cavity; hence, altering the directional couplers changes multiple characteristics of the transmission response, limiting the design flexibility. In the IMRR, we have the flexibility to change the bus-cavity coupling using any generic directional-coupling scheme, while simultaneously adjusting the power-splitting ratio between the two arms of the interferometer, as shown in the results of various devices in Fig. 3. The placement of the interferometer also affects the applications of the device. The transmission response of our structure has remarkable similarity with that of an ordinary microring resonator [see Eqs. (S6) and (S7) within the Supplemental Material [47]]. Hence, our structure can be more readily used in almost any application of the microring resonator, including higher-order reconfigurable filter synthesis, higher-order cascaded

TABLE I. Comparison of works on independent control of cavity resonance and dissipation of an optical cavity.

Key	[18]	[33–35]	Our work (IMRR)
Cavity type	Standing wave	Traveling wave	Traveling wave
Type of dissipation controlled	External loss through grating mirrors	External bus-cavity coupling loss	Internal cavity loss
Phase-tuning method	Local electro-optic/all-optical tuning; thermo-optics is challenging	Any method	Any method
Fabrication overhead	p - n junctions required for electro-optics	Overhead depends on tuning method used (no intrinsic overhead)	Overhead depends on the tuning method used (no intrinsic overhead)
ΔER at fixed resonance	10 dB	Not demonstrated (theoretically possible)	>20 dB (depends on proximity to critical coupling)
Broadband phase shift during phase tuning	Unknown	Yes	No
Required no. of control electrodes/knobs for resonance-locked operation	≥ 3	≤ 2	≤ 2
Max. no. of optical design parameters	3	6	8
Scalability to higher-order reconfigurable cavities	Simple	Challenging	Simple

reconfigurable resonators, cavity optomechanics, photonic cavity molecules, etc. [6–11,48].

In our experiments and simplified theoretical analysis, we consider the phases ϕ and δ as wavelength-independent parameters for a single optical resonance. However, we note that we are using an index-tuning approach to alter the phases. Therefore, both ϕ and δ are wavelength dependent and simultaneous locking of multiple resonances to get results similar to Fig. 4(e) for all resonances is challenging. Furthermore, the chromatic dispersion of the refractive index inhibits such performance. We also consider the geometric lengths of the two arms of the interferometer to be the same. Having a different geometric length of the two arms of the interferometer would also produce similar results, but has two important consequences. Firstly, it produces a phase offset between the two combining waves, which shifts only the quasiperiodic curves shown in Fig. 3; such a shift can be helpful in engineering the cavity loss and resonance shift at zero applied phase shift. Secondly, it also changes the relative magnitudes of the two combining fields due to unequal propagation loss in the two arms, thus adding a constant loss in the magnitude of the combined field. This effect is similar to a lossy directional-coupler based splitter and combiner, as is also encountered in the two-point coupled microring resonator [33–35]. It can also be used to engineer the device response such as the background loss in the cavity, irrespective of the applied phase shift. We have taken both these effects into consideration in our derivation within the Supplemental Material [47]. Both of these effects alter the quasiperiodic variation of

loss and resonance shift in the device, but do not impede the functionality of the device in achieving results similar to Fig. 4.

In conclusion, we show that embedding an interferometer within a traveling-wave optical cavity enables complete reconfiguration of the internal loss, resonant wavelength, transmission characteristics, and group delay of the cavity. We also demonstrate that the interferometer can be engineered to achieve the desired quasiperiodic modifications in the loss and the resonant wavelength. This structure provides a unique method to achieve both blue- and redshifts of the cavity resonance by the same phase-tuning mechanism. In the context of thermo-optic tuning, it implies that irrespective of the sign of the thermo-optic coefficient of the waveguide material (such as positive for silicon), one can observe both thermo-optic blueshift and redshift of the resonance, which is a useful asset for universal reconfigurable cavities. Another advantage of the interferometer-embedded cavity is that the internal loss can be tuned independent of the resonance shift by simultaneously tuning the phases in both arms of the interferometer. This offers the practical advantage of tuning the parameters related to loss such as Q factor, ER, and group-delay while still operating at the same resonant frequency (wavelength). The generic structure can be implemented in any guided-wave platform, such as integrated photonics or fiber optics. Exotic photonic material platforms, such as lithium niobate and boron nitride, can benefit from this structure in applications, such as optical modulation, nonlinear optics, and quantum optics [55,56]. While it can also

be implemented in free space, the reflections induced by destructive interference in the MZI need to be carefully addressed. The versatility of the IMRR makes it a promising candidate for reconfigurable photonics and photonic signal processing and opens up a set of tools for cavity optomechanics and optomechanical memories.

ACKNOWLEDGMENT

We acknowledge financial support from Ministry of Education, India through Grant No. MOE-STARS/APR2019/534. We also acknowledge funding from MHRD, MeitY and DST Nano Mission for supporting the facilities at Centre for Nano Science and Engineering.

-
- [1] J. Li, H. Lee, T. Chen, and K. J. Vahala, Characterization of a high coherence, Brillouin microcavity laser on silicon, *Opt. Express* **20**, 20170 (2012).
- [2] I. S. Grudinin, A. B. Matsko, and L. Maleki, Brillouin Lasing with a CaF₂ Whispering Gallery Mode Resonator, *Phys. Rev. Lett.* **102**, 043902 (2009).
- [3] B. Yao, S.-W. Huang, Y. Liu, A. K. Vinod, C. Choi, M. Hoff, Y. Li, M. Yu, Z. Feng, D.-L. Kwong, Y. Huang, Y. Rao, X. Duan, and C. W. Wong, Gate-tunable frequency combs in graphene-nitride microresonators, *Nature* **558**, 410 (2018).
- [4] S. Ramelow, A. Farsi, Z. Vernon, S. Clemmen, X. Ji, J. E. Sipe, M. Liscidini, M. Lipson, and A. L. Gaeta, Strong Non-linear Coupling in a Si₃N₄ Ring Resonator, *Phys. Rev. Lett.* **122**, 153906 (2019).
- [5] M. T. M. Woodley, L. Hill, L. Del Bino, G. L. Oppo, and P. Del'Haye, Self-Switching Kerr Oscillations of Counter-propagating Light in Microresonators, *Phys. Rev. Lett.* **126**, 043901 (2021).
- [6] T. Kippenberg and K. Vahala, Cavity opto-mechanics, *Opt. Express* **15**, 17172 (2007).
- [7] T. J. Kippenberg and K. J. Vahala, Cavity optomechanics: Back-action at the mesoscale, *Science* **321**, 1172 (2008).
- [8] G. Anetsberger, R. Rivière, A. Schliesser, O. Arcizet, and T. J. Kippenberg, Ultralow-dissipation optomechanical resonators on a chip, *Nat. Photonics* **2**, 627 (2008).
- [9] G. Anetsberger, O. Arcizet, Q. P. Unterreithmeier, R. Rivière, A. Schliesser, E. M. Weig, J. P. Kotthaus, and T. J. Kippenberg, Near-field cavity optomechanics with nanomechanical oscillators, *Nat. Phys.* **5**, 909 (2009).
- [10] S. Weis, R. Rivière, S. Deléglise, E. Gavartin, O. Arcizet, A. Schliesser, and T. J. Kippenberg, Optomechanically induced transparency, *Science* **330**, 1520 (2010).
- [11] M. Aspelmeyer, T. J. Kippenberg, and F. Marquardt, in *Cavity Optomechanics Nano- and Micromechanical Resonators Interacting with Light*, edited by M. Aspelmeyer, T. J. Kippenberg, and F. Marquardt (Springer, Berlin, Heidelberg, 2014), p. 1.
- [12] P. R. Prasad, S. K. Selvaraja, and M. M. Varma, High precision measurement of intensity peak shifts in tunable cascaded microring intensity sensors, *Opt. Lett.* **41**, 3153 (2016).
- [13] A. Dash, S. K. Selvaraja, and A. K. Naik, On-chip optical transduction scheme for graphene nano-electro-mechanical systems in silicon-photonics platform, *Opt. Lett.* **43**, 659 (2018).
- [14] B. E. Little, S. T. Chu, H. A. Haus, J. Foresi, and J. Laine, Microring resonator channel dropping filters, *J. Light. Technol.* **15**, 998 (1997).
- [15] T. Yang, J. Dong, L. Liu, S. Liao, S. Tan, L. Shi, D. Gao, and X. Zhang, Experimental observation of optical differentiation and optical Hilbert transformation using a single SOI microdisk chip, *Sci. Rep.* **4**, 3960 (2015).
- [16] Y. Park, J. Azaña, and R. Slavík, Ultrafast all-optical first- and higher-order differentiators based on interferometers, *Opt. Lett.* **32**, 710 (2007).
- [17] M. Rasras, Kun-Yii Tu, D. Gill, Young-Kai Chen, A. White, S. Patel, A. Pomerene, D. Carothers, J. Beattie, M. Beals, J. Michel, and L. Kimerling, Demonstration of a tunable microwave-photonics notch filter using low-loss silicon ring resonators, *J. Light. Technol.* **27**, 2105 (2009).
- [18] W. Zhang and J. Yao, A fully reconfigurable waveguide Bragg grating for programmable photonic signal processing, *Nat. Commun.* **9**, 1396 (2018).
- [19] D. A. B. Miller, Reconfigurable add-drop multiplexer for spatial modes, *Opt. Express* **21**, 20220 (2013).
- [20] H. Haus, M. Popovic, and M. Watts, Broadband hitless bypass switch for integrated photonic circuits, *IEEE Photonics Technol. Lett.* **18**, 1137 (2006).
- [21] M. A. Popović, E. P. Ippen, and F. X. Kärtner, Universally balanced photonic interferometers, *Opt. Lett.* **31**, 2713 (2006).
- [22] W. Bogaerts, D. Pérez, J. Capmany, D. A. B. Miller, J. Poon, D. Englund, F. Morichetti, and A. Melloni, Programmable photonic circuits, *Nature* **586**, 207 (2020).
- [23] X. Chen, P. Stroobant, M. Pickavet, and W. Bogaerts, Graph representations for programmable photonic circuits, *J. Light. Technol.* **38**, 4009 (2020).
- [24] A. Ribeiro, S. Declercq, U. Khan, M. Wang, L. V. Iseghem, and W. Bogaerts, Column-row addressing of thermo-optic phase shifters for controlling large silicon photonic circuits, *IEEE J. Sel. Top. Quantum Electron.* **26**, 1 (2020).
- [25] A. Dash, V. Mere, P. R. Y. Gangavarapu, S. R. Nambiar, S. K. Selvaraja, and A. K. Naik, Carbon-nanotube-on-waveguide thermo-optic tuners, *Opt. Lett.* **43**, 5194 (2018).
- [26] A. Masood, M. Pantouvaki, D. Goossens, G. Lepage, P. Verheyen, J. V. Campenhout, P. Absil, D. V. Thourhout, and W. Bogaerts, Fabrication and characterization of CMOS-compatible integrated tungsten heaters for thermo-optic tuning in silicon photonics devices, *Opt. Mater. Express* **4**, 1383 (2014).
- [27] H. Du, X. Zhang, C. G. Littlejohns, D. T. Tran, X. Yan, M. Banakar, C. Wei, D. J. Thomson, and G. T. Reed, Nonconservative Coupling in a Passive Silicon Microring Resonator, *Phys. Rev. Lett.* **124**, 013606 (2020).
- [28] L. A. Shiramin and D. V. Thourhout, Graphene modulators and switches integrated on silicon and silicon nitride waveguide, *IEEE J. Sel. Top. Quantum Electron.* **23**, 94 (2017).
- [29] Y. Ding, X. Zhu, S. Xiao, H. Hu, L. H. Frandsen, N. A. Mortensen, and K. Yvind, Effective electro-optical modulation with high extinction ratio by a graphene-silicon microring resonator, *Nano Lett.* **15**, 4393 (2015).

- [30] L. Alloatti, D. Korn, R. Palmer, D. Hillerkuss, J. Li, A. Barklund, R. Dinu, J. Wieland, M. Fournier, J. Fedeli, H. Yu, W. Bogaerts, P. Dumon, R. Baets, C. Koos, W. Freude, and J. Leuthold, 427 Gbit/s electro-optic modulator in silicon technology, *Opt. Express* **19**, 11841 (2011).
- [31] A. Dash, U. Palanchoke, M. Gely, G. Jourdan, S. Hentz, S. K. Selvaraja, and A. K. Naik, Enhanced all-optical cavity-tuning using graphene, *Opt. Express* **27**, 34093 (2019).
- [32] A. Pandey and S. K. Selvaraja, Broadly tunable and low power penalty radio frequency phase shifter using a coupled silicon microcavity, *Appl. Opt.* **59**, 425 (2020).
- [33] D. Aguiar, M. Milanizadeh, E. Guglielmi, F. Zanetto, R. Ji, S. Zhou, Y. Li, X. Song, L. Zhang, M. Sampietro, F. Morichetti, and A. Melloni, in *Optical Fiber Communication Conference* (Optica Publishing Group, San Diego, 2018), p. W2A.41.
- [34] H. Shoman, H. Jayatilleka, N. A. F. Jaeger, S. Shekhar, and L. Chrostowski, Measuring on-chip waveguide losses using a single, two-point coupled microring resonator, *Opt. Express* **28**, 10225 (2020).
- [35] F. Morichetti, M. Milanizadeh, M. Petrini, F. Zanetto, G. Ferrari, D. O. de Aguiar, E. Guglielmi, M. Sampietro, and A. Melloni, Polarization-transparent silicon photonic add-drop multiplexer with wideband hitless tuneability, *Nat. Commun.* **12**, 4324 (2021).
- [36] W. Liu, M. Li, R. S. Guzzon, E. J. Norberg, J. S. Parker, M. Lu, L. A. Coldren, and J. Yao, A fully reconfigurable photonic integrated signal processor, *Nat. Photonics* **10**, 190 (2016).
- [37] Y. Xie, Y. Shi, L. Liu, J. Wang, R. Priti, G. Zhang, O. Liboiron-Ladouceur, and D. Dai, Thermally-reconfigurable silicon photonic devices and circuits, *IEEE J. Sel. Top. Quantum Electron.* **26**, 1 (2020).
- [38] H. Zhou, Y. Zhao, X. Wang, D. Gao, J. Dong, and X. Zhang, Self-configuring and reconfigurable silicon photonic signal processor, *ACS Photonics* **7**, 792 (2020).
- [39] G. Sinatkas, T. Christopoulos, O. Tsilipakos, and E. E. Kriezis, Electro-optic modulation in integrated photonics, *J. Appl. Phys.* **130**, 010901 (2021).
- [40] K. J. Miller, R. F. Haglund, and S. M. Weiss, Optical phase change materials in integrated silicon photonic devices: review, *Opt. Mater. Express* **8**, 2415 (2018).
- [41] V. Jeyaselvan, A. Pal, P. S. Anil Kumar, and S. K. Selvaraja, Thermally-induced optical modulation in a vanadium dioxide-on-silicon waveguide, *OSA Contin.* **3**, 132 (2020).
- [42] P. Orlandi, F. Morichetti, M. J. Strain, M. Sorel, A. Melloni, and P. Bassi, Tunable silicon photonics directional coupler driven by a transverse temperature gradient, *Opt. Lett.* **38**, 863 (2013).
- [43] D. Pérez-López, A. M. Gutierrez, E. Sánchez, P. DasMahapatra, and J. Capmany, Integrated photonic tunable basic units using dual-drive directional couplers, *Opt. Express* **27**, 38071 (2019).
- [44] H. Sattari, A. Y. Takabayashi, Y. Zhang, P. Verheyen, W. Bogaerts, and N. Quack, Compact broadband suspended silicon photonic directional coupler, *Opt. Lett.* **45**, 2997 (2020).
- [45] T. J. Seok, N. Quack, S. Han, R. S. Muller, and M. C. Wu, Large-scale broadband digital silicon photonic switches with vertical adiabatic couplers, *Optica* **3**, 64 (2016).
- [46] Y. Long and J. Wang, Optically-controlled extinction ratio and Q-factor tunable silicon microring resonators based on optical forces, *Sci. Rep.* **4**, 5409 (2015).
- [47] See Supplemental Material at <http://link.aps.org/supplemental/10.1103/PhysRevApplied.18.054032>, for details of device fabrication, additional data, methods, and derivation of equations.
- [48] A. Tikan, J. Riemensberger, K. Komagata, S. Hönl, M. Churaev, C. Skehan, H. Guo, R. N. Wang, J. Liu, P. Seidler, and T. J. Kippenberg, Emergent nonlinear phenomena in a driven dissipative photonic dimer, *Nat. Phys.* **17**, 604 (2021).
- [49] V. Mere, R. Kallega, and S. K. Selvaraja, Efficient and tunable strip-to-slot fundamental mode coupling, *Opt. Express* **26**, 438 (2018).
- [50] *Integrated Ring Resonators: The Compendium*, edited by D. G. Rabus (Springer, Berlin, Heidelberg, 2007), p. 3.
- [51] J. E. Heebner, V. Wong, A. Schweinsberg, R. W. Boyd, and D. J. Jackson, Optical transmission characteristics of fiber ring resonators, *IEEE J. Quantum Electron.* **40**, 726 (2004).
- [52] B. Jin, J. Yuan, K. Wang, X. Sang, B. Yan, Q. Wu, F. Li, X. Zhou, G. Zhou, C. Yu, C. Lu, H. Yaw Tam, and P. K. Wai, A comprehensive theoretical model for on-chip microring-based photonic fractional differentiators, *Sci. Rep.* **5**, 1 (2015).
- [53] L. Zhou, X. Sun, J. Xie, Z. Zou, L. Lu, and J. Chen, Characterisation of microring resonator optical delay and its dependence on coupling gap using modulation phase-shift technique, *Electron. Lett.* **48**, 1613 (2012).
- [54] F. Liu, T. Wang, L. Qiang, T. Ye, Z. Zhang, M. Qiu, and Y. Su, Compact optical temporal differentiator based on silicon microring resonator, *Opt. Express* **16**, 15880 (2008).
- [55] V. Mere, F. Valdez, X. Wang, and S. Mookherjee, A modular fabrication process for thin-film lithium niobate modulators with silicon photonics, *J. Phys. Photonics* **4**, 024001 (2022).
- [56] C. Li, J. E. Fröch, M. Nonahal, T. N. Tran, M. Toth, S. Kim, and I. Aharonovich, Integration of hBN quantum emitters in monolithically fabricated waveguides, *ACS Photonics* **8**, 2966 (2021).